ACS APPLIED MATERIALS & INTERFACES

Research Article

www.acsami.org

Optical Gas Sensing Properties of Nanoporous Nb_2O_5 Films

Rosmalini Ab Kadir,*[,†,⊥] Rozina Abdul Rani,[†] Manal M. Y. A. Alsaif,[†] Jian Zhen Ou,[†] Wojtek Wlodarski,[†] Anthony P. O'Mullane,[‡] and Kourosh Kalantar-zadeh*[,†]

[†]School of Electrical and Computer Engineering, RMIT University, Melbourne, Victoria 3001, Australia

[‡]School of Chemistry, Physics and Mechanical Engineering, Queensland University of Technology, Brisbane, Queensland 4001, Australia

[⊥]Faculty of Electrical Engineering, MARA University of Technology, 40450 Shah Alam, Selangor, Malaysia

Supporting Information

ABSTRACT: Nanoporous Nb_2O_5 has been previously demonstrated to be a viable electrochromic material with strong intercalation characteristics. Despite showing such promising properties, its potential for optical gas sensing applications, which involves the production of ionic species such as H^+, has yet to be explored. Nanoporous Nb_2O_5 can accommodate a large amount of H^+ ions in a process that results in an energy bandgap change of the material which induces an optical response. Here, we demonstrate the optical hydrogen gas (H_2) sensing capability of nanoporous anodic Nb_2O_5 with a large surface-to-volume ratio prepared via a high temperature anodization method. The large active surface area of the film provides enhanced pathways for efficient hydrogen adsorption and dissociation, which are facilitated by a thin layer of Pt catalyst. We show that the process of H_2 sensing causes optical modulations that are investigated in terms of response magnitudes and dynamics. The optical modulations induced by the intercalation process and sensing properties of nanoporous anodic Nb_2O_5 shown in this work can potentially be used for future optical gas sensing systems.

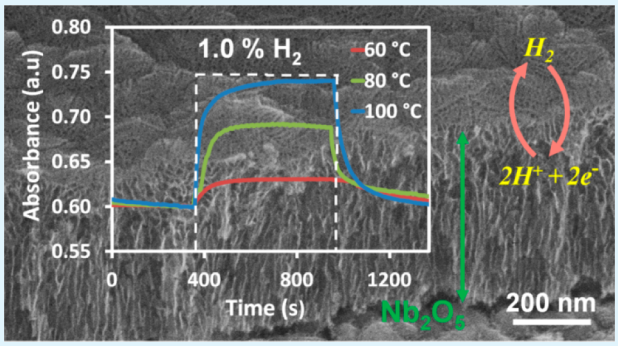

KEYWORDS: *niobium oxide (Nb_2O_5), anodization, nanoporous, optical response, hydrogen, gas sensing*

1. INTRODUCTION

Metal oxide semiconductors such as WO_3, NiO, and MoO_3 are known for their outstanding performance as electro- and chemochromic materials due to their unique properties.[1−10] Developments of electrochromic devices and chemochromic optical sensors have been prompted by their ability to reversibly change their transmittance, absorption, and reflectance according to applied voltages and ambient conditions. These materials generally change their color and transparency as a result of the intercalation of ionic species such as Li^+ and H^+, which alter their electronic band structure.[11]

Among the intercalatable metal oxide semiconductors, Nb_2O_5 is one of the emerging but less studied oxides. Nb_2O_5 has been demonstrated to have excellent optical properties, outstanding electrochemical responses, chemical stability, corrosion resistance, and coloration changes.[12−14] Crystalline Nb_2O_5 has low electrical conductivity of $\sim 10^{-6}$ S cm^{-1}, which is at least 2 orders of magnitude smaller in comparison to its electrochromic metal oxide counterparts such as MoO_3 and WO_3.[15] It has been shown that upon intercalation of ionic species, crystalline Nb_2O_5 exhibits a color change from transparent to blue, while amorphous Nb_2O_5 changes into a brownish-gray color.[14] Intercalation also results in optical modulation. However, in electrochromic applications, the optical modulation performance of amorphous Nb_2O_5 films rapidly degrades compared to crystalline films.[16−18]

Considering the aforementioned characteristics of crystalline Nb_2O_5, there are significant opportunities for developing optical gas sensing elements based on this metal oxide. A critical approach in creating effective Nb_2O_5 based gas sensors is to form nanomorphologies of this material that allow facile adsorption and dissociation of target gas molecules. Nanostructured Nb_2O_5 materials have been fabricated using various methods in order to obtain high specific surface area and controllable structures. Liquid phase deposition methods such as hydrothermal and solvothermal routes have produced Nb_2O_5 with various morphologies comprising of nanobelts, nanospheres, nanosheets, and nanorods.[19−24] In addition, nanoporous, nanochannelled, nanoveined, and nanocolumns of Nb_2O_5 have also been synthesized via electrochemical methods.[25−30] Among these methods, anodization is a particularly interesting technique due to its capability of forming highly porous films. Such structures provide platforms for efficient gas molecule diffusion, resulting in a high optical response and therefore augment a sensors' performance.

Received: December 2, 2014
Accepted: February 16, 2015
Published: February 16, 2015

DOI: 10.1021/am508463g
ACS Appl. Mater. Interfaces 2015, 7, 4751−4758

In our previous work, we demonstrated an enhanced coloration efficiency of 47.0 cm^2 C^{-1} for crystalline nanoporous anodic Nb_2O_5, which is to date the highest ever reported for any electrochromic Nb_2O_5 based system.[13] In this work, we demonstrated the possibility of intercalating a large amount of Li^+ ions into nanoporous anodic Nb_2O_5, with high surface-to-volume ratios, at very low applied voltages. Based on the excellent electrochromic performance of these Nb_2O_5 structures, it is proposed that crystalline nanoporous anodic Nb_2O_5 can also be a suitable candidate for optical gas sensing. The breakdown of the hydrogen molecule onto the surface of nanoporous anodic Nb_2O_5, with or without the assistance of a catalyst, can be used for producing H^+ ions that intercalate the crystal. These H^+ ions can subsequently change the electronic band structure of nanoporous anodic Nb_2O_5 generating a different optical response. It is known that in metal oxides with a propensity for intercalation, Li^+ and H^+ ions generally reduce the bandgap and eventually produce semimetallic compounds for strongly intercalated systems.[31−35] Consequently, it is proposed that hydrogen containing gas molecules are also able to reduce the energy bandgap of Nb_2O_5 to produce measurable optical modulations. However, the optical gas sensing properties of Nb_2O_5 have not been studied. Hydrogen gas (H_2) is an excellent model to investigate this hypothesis. The applications of H_2 gas span from industrial surveillance and processes to fuel cells, petroleum refining, airspace, and biomedical systems.[36−40] H_2 gas is a colorless, odorless, explosive, and extremely flammable gas. Therefore, H_2 leakage monitoring is paramount for its safe production, storage, handling, and use.

In this work, we investigate the optical sensing performance of a nanoporous anodic Nb_2O_5 film in the presence of H_2. Nanoporous Nb_2O_5 films are prepared by anodization of Nb metal films, which are deposited using RF sputtering onto fluorine-doped tin oxide (FTO) glass substrates. Anodization of Nb using an electrolyte containing glycerol and dipotassium phosphate (K_2HPO_4) at elevated temperature has been demonstrated by Melody et al.[41] to produce nanoporous Nb_2O_5 films. This electrolyte composition has been identified as having low resistivity and thermal stability that contributes to the formation of porous films.[42] It has been proved that anodization at high temperatures with the electrolyte of glycerol/dipotassium phosphate, accelerates the process and results in much more robust and highly ordered nanoporous films.[42−45] In this work, the same electrolyte is used for the formation of the nanoporous anodic Nb_2O_5 films. Experiments are conducted in order to assess the crystalline and morphological properties of Nb_2O_5 films and to reveal the subsequent optical changes, which occur upon hydrogen gas molecule interactions with these films. Responses of the films to methane and ethanol gas molecules are also investigated for comparison.

2. EXPERIMENTAL SECTION

2.1. Synthesis of Nb_2O_5. The Nb films used in this work were prepared by a RF magnetron sputtering system. Fluorine-doped tin oxide (15 Ω sq^{-1}, Dyesol) glass substrates measuring 15 mm × 10 mm were used. Nb films were deposited by means of a RF magnetron sputtering using a circular metallic Nb target of 2 in. in diameter with a purity of 99.95% placed at a distance of 65 mm from the substrate stage. The base pressure of the sputtering chamber was 1.0×10^{-5} Torr, and the sputtering pressure was set to 2×10^{-2} Torr in the presence of pure argon (100%). A constant 120 W RF power was used with the substrate temperature fixed at 300 °C for 20 min of sputtering. The sputtering process utilizing the aforementioned parameters resulted in Nb metal films of ∼350 nm thicknesses. The sputtered Nb films were anodized in an electrolyte that consisted of 50 mL glycerol (99% purity) mixed with 6.3 g of K_2HPO_4 (98% purity) (both from Sigma−Aldrich) that was kept at a constant temperature of 180 °C during the anodization process. The anodization was carried out with a conventional two electrode configuration, where the anode was the sample and the cathode was a Pt foil. The anodization duration of 3 min at a voltage of 5 V resulted in nanoporous Nb_2O_5 films of ∼500 nm thicknesses. The films were then washed using deionized water and dried in a nitrogen stream. The samples were then annealed in a standard laboratory furnace at 500 °C for 1 h in air with a ramp-up and ramp-down rate of 2 °C min^{-1} which resulted in transparent crystalline nanoporous Nb_2O_5 films. A Pt catalytic layer of ∼1 nm thickness was sputtered onto the film surface to facilitate and enhance the breakdown of H_2 molecules. In our previous work, the as-synthesized compact Nb_2O_5 nanoporous films with a thickness of 500 nm demonstrated the optimum coloration efficiency in electrochromic applications.[13] As such, we chose this thickness for our optical gas sensing investigations.

2.2. Structural Characterizations. The scanning electron microscopy (SEM) images of the Nb_2O_5 films were taken with a FEI Nova NanoSEM, while the elemental composition of the Nb and Nb_2O_5 films were examined by X-ray photoemission spectroscopy (XPS) using a Thermo K-alpha X-ray source (1486.7 eV) at 50 eV pass energy. The crystalline structure of the Nb_2O_5 films were determined by X-ray diffraction (XRD), characterized by a D8 Advance Bruker AXS with General Area Detector Diffraction System (GADDS) attachment fitted with a 50 μm spot size collimator, incorporating a High Star 2-dimensional detector and CuKα radiation (λ = 0.1542 nm) operating at 40 kV and 40 mA. Raman spectra were obtained using an Ocean Optic QE 6500 spectrometer, equipped with a 532 nm 40 mW laser as the excitation source.

2.3. Optical Gas Sensing Measurements. The absorption spectra of the nanoporous Nb_2O_5 films were examined using the testing setup shown in Figure S1 (Supporting Information). The custom-made chamber (Figure 1 shows the schematic illustration) consisted of an aluminum box with ports for a gas inlet and outlet, ports for light to pass through, and electrical connectors for a heating plate. The optical signal was provided using a deuterium-halogen single beam light source (Micropack DH-200) and measured by a spectrophotometer (Ocean Optics HR 4000). A custom built sample holder was utilized to mount the sensing elements during testing. The operating temperatures of these sensing elements were regulated using a localized heater, which was connected to a dc voltage supply. The hydrogen gas was pulsed into the inlets of the aluminum box where the concentration was accurately controlled using a computerized mass flow control (MFC) multichannel gas calibration system. Exposure time was 10 min for each pulse of hydrogen gas, and the chamber was purged with synthetic air for 10 min between pulses to allow the sensors to recover under atmospheric conditions. The analysis was performed using Spectrasuite Software Package.

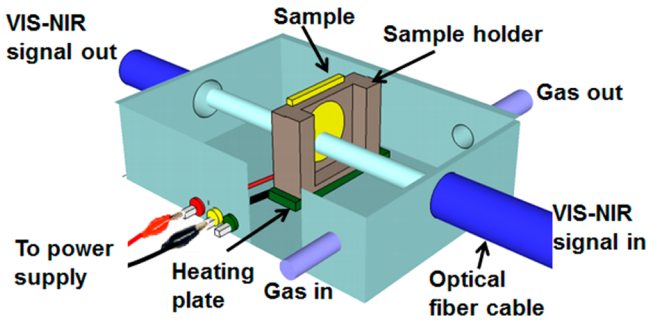

Figure 1. A schematic illustration of the optical gas testing chamber.

DOI: 10.1021/am508463g
ACS Appl. Mater. Interfaces 2015, 7, 4751−4758

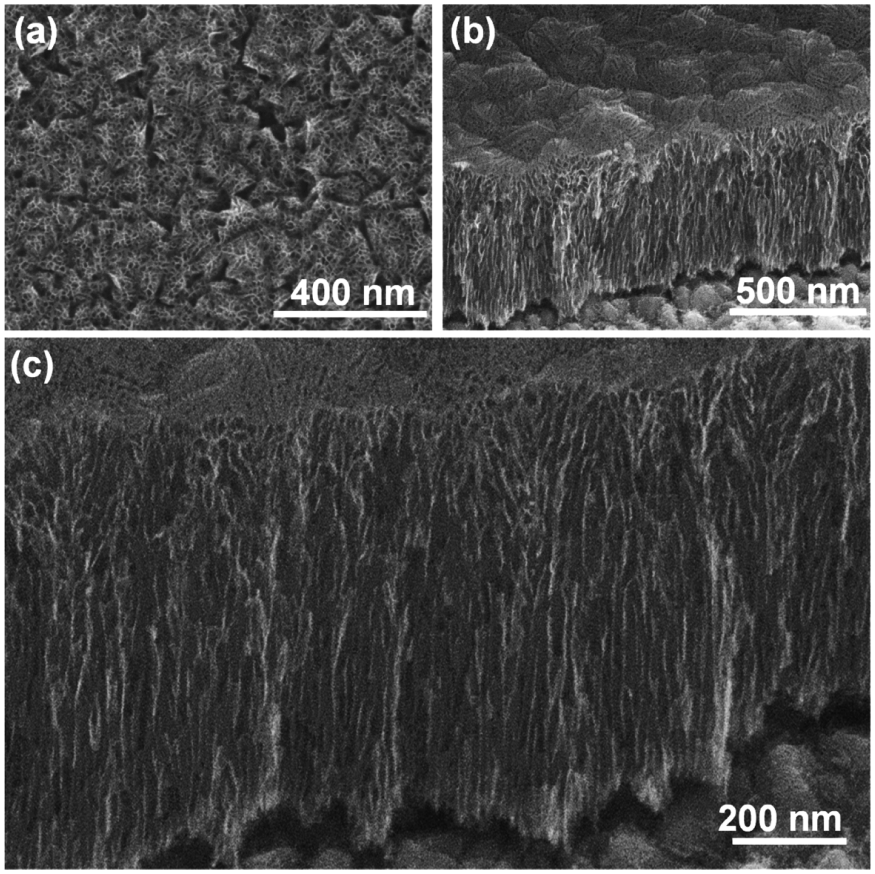

Figure 2. SEM images of (a) top view, (b) cross-sectional view, and (c) magnified image of the cross-sectional view of nanoporous anodic Nb_2O_5.

3. RESULTS AND DISCUSSION

3.1. Morphological and Structural Properties. The surface and cross-sectional SEM images of nanoporous anodic Nb_2O_5 films are presented in Figure 2. From the top-view SEM image of the nanoporous anodic Nb_2O_5 layer in Figure 2(a), it can be seen that apart from the large pores with an average dimension of ~35 nm, smaller pores with sizes ranging from 10 to 15 nm were also formed throughout the films, thus making all of the pores connected into a three-dimensional (3D) porous nanostructure. From the cross-sectional images depicted in Figure 2(b,c), it is observed that the anodized thin films are composed of arrays of continuous and high density nanoporous networks that are ordered in vertical directions. The observation of such a nanoporous structure proves the efficiency of the adopted anodization process in establishing an efficient sensing element for the adsorption and diffusion of gas molecules.

An XPS analysis was carried out to determine the elemental composition of the sputtered Nb and annealed nanoporous anodic Nb_2O_5 films. Figure 3(a) shows the zoomed in spectrum of the Nb region of the sputtered Nb film. The spectrum exhibits the Nb $3d_{3/2}$ peak at 205.8 eV and Nb $3d_{5/2}$ at 202.3 eV. This spectrum indicates that the film is made of pure Nb according to Dacca et al.[46] As shown in Figure 3(b), the zoomed in spectrum of Nb_2O_5 contains peaks at 207.3 and 210.1 eV, which are accredited to the Nb $3d_{5/2}$ and Nb $3d_{3/2}$ energy levels, respectively. These peaks are evidence of the formation of Nb_2O_5 after annealing.[13]

XRD measurements were carried out to examine the crystalline structures of the as-anodized and annealed Nb_2O_5.

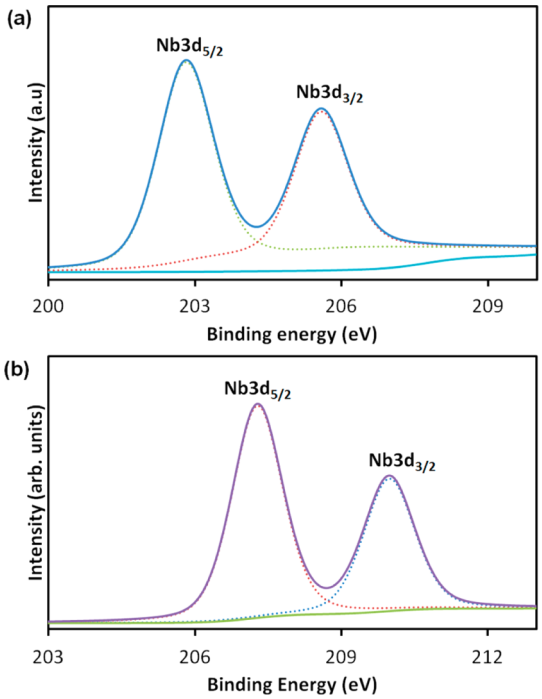

Figure 3. XPS spectra of Nb 3d peaks of (a) sputtered Nb and (b) nanoporous anodic Nb_2O_5 films (both XPS spectra are calibrated with reference to peak fitting of the carbon 1s peak located at 284.5 eV (not shown)).

DOI: 10.1021/am508463g
ACS Appl. Mater. Interfaces 2015, 7, 4751−4758

The XRD patterns of the as-anodized sample (Figure 4-i) display only Nb peaks together with the FTO peaks, indicating

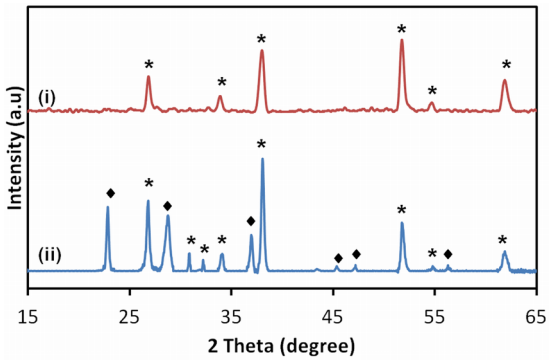

Figure 4. XRD patterns of nanoporous Nb_2O_5 film (i) as anodized and (ii) after annealing in air for 1 h at 500 °C, orthorhombic phase (ICDD27-1003) peaks are denoted by ♦, while FTO peaks are denoted by *.

the amorphous nature of the films. The films were crystalline and formed the orthorhombic phase of Nb_2O_5 (according to ICDD27-1003) after 1 h of annealing at a temperature of 500 °C as indicated by peaks appearing at 22.6, 28.5, 37.0, 45.0, 46.3, and 55.5° 2-theta (Figure 4-ii).[26]

The XRD results were further verified by the Raman spectra presented in Figure 5. The broad peaks at 250 and 650 cm^{-1}

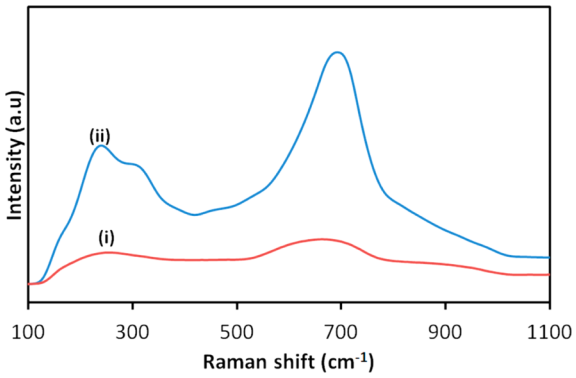

Figure 5. Raman spectra of (i) as-anodized and (ii) nanoporous anodic Nb_2O_5 films annealed at 500 °C for 1 h in air.

were observed in the spectrum of the as-deposited nanoporous films signifying the characteristics of amorphous niobium oxide. After annealing, the Raman peaks for the nanoporous Nb_2O_5 were clearly visible by peaks located at 250, 303, and 690 cm^{-1}. These peak positions correspond to the orthorhombic phase of crystalline Nb_2O_5 as previously reported.[13,47] The XRD and Raman analysis both confirm the orthorhombic phase of the nanoporous anodic Nb_2O_5 film.

3.2. Optical Gas Sensing Assessments. The optical response of the nanoporous anodic Pt/N_2O_5 film to hydrogen gas was first investigated under different operating temperatures. The measurements were conducted at 22, 40, 60, 80, and 100 °C by exposing it alternately to synthetic air and 1% hydrogen gas in air. Temperatures above 100 °C were not implemented as the test chamber could not withstand such elevated temperatures. It was found that the Pt/Nb_2O_5 film did not show any distinguishable gas response at room temperature as shown in Figure 6(a). It is suggested that at such a low

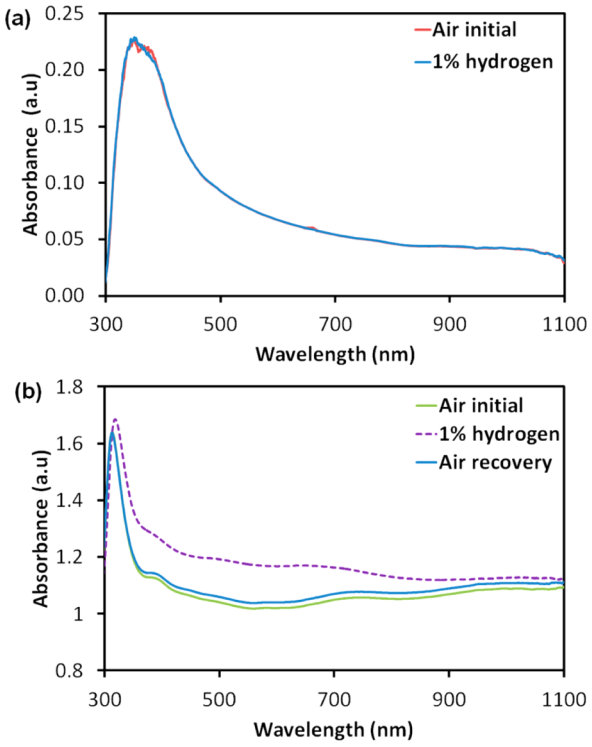

Figure 6. Absorbance versus optical wavelength spectra for nanoporous anodic Pt/Nb_2O_5 films exposed to 1% H_2 at (a) room temperature and (b) 100 °C.

temperature, there is insufficient energy for the hydrogen gas molecules to dissociate. This can be ascribed to the wide band gap and high conduction band edge of Nb_2O_5.[13]

The exposure of 1% hydrogen gas to the Pt/Nb_2O_5 films at 100 °C resulted in a change of the absorption spectrum over a wide wavelength range from 350 to 900 nm (Figure 6(b)). At the elevated temperature of 100 °C, the adsorption rate of H^+ ions increases due to sufficient energy being available to dissociate molecular hydrogen, while at the same time the formation of water vapor on the surface becomes limited, which would increase the efficient surface area available for the gas adsorption response.[26,29,48,49] Good reversibility is also observed at the 100 °C operating temperature.

The optical absorption properties of nanoporous anodic Nb_2O_5 films are tuned by the intercalation of H^+ ions that resulted from the dissociation of hydrogen gas molecules in the presence of the Pt catalyst. These reactions alter the electronic band structure of the Nb_2O_5 films,[13] which consequently changes the optical absorbance of the films. The detailed mechanism of optical hydrogen gas sensing using nanoporous anodic Nb_2O_5 is discussed in details as follows.

Hydrogen gas dissociates on the Pt catalyst forming hydrogen ions (H^+) and electrons (e^-):[50]

$$H_2(g) \rightarrow 2H^+ + 2e^- \quad (1)$$

The generated hydrogen ions and electrons are simultaneously intercalated into the nanoporous anodic Nb_2O_5 film. Gradually water molecules (H_2O) are formed via the reduction of Nb_2O_5 to $Nb_2O_{5-x/2}$ as described by the following reactions:[13,26]

$$Nb_2O_5 + xH^+ + xe^- \rightleftharpoons H_xNb_2O_5 \quad (2)$$

DOI: 10.1021/am508463g
ACS Appl. Mater. Interfaces 2015, 7, 4751−4758

$$2H_xNb_2O_5 \rightleftharpoons xH_2O + Nb_2O_{5-x/2} \quad (3)$$

It is suggested NbO_2 is formed for the case of $x = 2$.[29] According to eq 2, the intercalated H^+ ions are embedded into the crystal structure of Nb_2O_5. The released electrons are transferred to the lowest-lying unoccupied energy levels of Nb_2O_5.[13] Thus, the stoichiometry of the nanoporous anodic film is changed, and its electronic band structure is altered, which results in an increase of the film absorbance. By purging the hydrogen gas source out of the system by exposing the films to air (oxygen rich environment) the adsorbed oxygen species restore the stoichiometry of the nanoporous anodic Nb_2O_5 films and hence reduce the level of absorbance to the original state as follows:[26]

$$Nb_2O_{5-x/2} + (x/4) \rightleftharpoons Nb_2O_5 \quad (4)$$

This indicates the reversibility of the chemical reactions and thereby justifies the use of this material in a repeatable manner as a gas sensing material.

As mentioned previously, the intercalation of H^+ ions reduces the bandgap of Nb_2O_5. The bandgap energies were calculated from the UV–vis absorption spectra shown in Figure 6(b) using the Tauc equation (see the Supporting Information for details).[2] It was found that the bandgap of the nanoporous anodic Nb_2O_5 film under ambient air exposure was 3.26 eV. The bandgap reduced to 2.99 eV in the presence of 1% hydrogen due to the intercalation of H^+ ions into the Nb_2O_5 film as described by eq 2.[32−35]

Figure 7 shows the dynamic response of the Pt/Nb_2O_5 films toward 1% hydrogen gas concentration at different operating

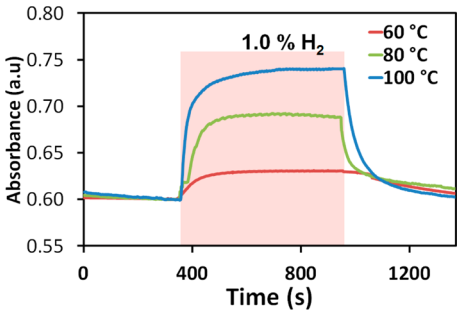

Figure 7. Dynamic responses of the nanoporous anodic Nb_2O_5 optical element under 1% hydrogen exposure at different temperatures recorded at a wavelength of 600 nm.

temperatures of 60, 80, and 100 °C. The measurements were carried out at a single wavelength of 600 nm, which was the wavelength where the maximum absorption was recorded in the visible region in Figure 6(b). As can be seen, the response magnitude increases by increasing the operating temperature. At low temperatures the dissociation of H_2 on Pt is suppressed, slowing the kinetics of e^- and H^+ injection into the nanoporous anodic Nb_2O_5 lattice. However, as the temperature increases, the response increases due to more efficient H_2 adsorption and dissociation on the catalyst surface and spill over into the Nb_2O_5 optical element.

Figure 8(a) shows the dynamic responses of the nanoporous anodic Pt/Nb_2O_5 films over a H_2 concentration range of 0.06 to 1.0%, measured at a single wavelength of 600 nm at 100 °C. It was found that the absorption change increases linearly with increasing hydrogen gas concentration as observed from the plot shown in Figure 8(b). With hydrogen gas concentrations

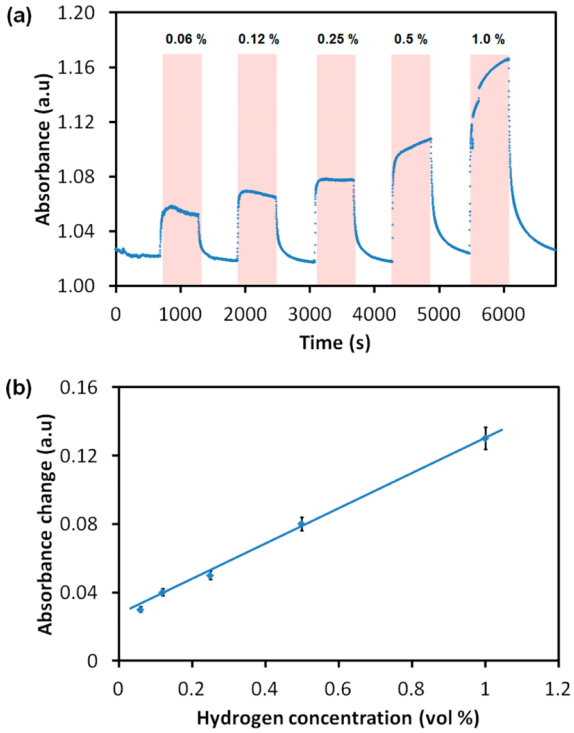

Figure 8. (a) Dynamic performance and (b) absorbance change of nanoporous anodic Pt/Nb_2O_5 films after exposure to different concentrations of hydrogen gas at 100 °C at the wavelength of 600 nm.

of 0.06, 0.12, 0.25, 0.5, and 1.0%, absorption changes of 0.03, 0.04, 0.05, 0.08, and 0.12 were recorded. When the gas supply was repeatedly switched from air to hydrogen gas (in air background), the baseline remained stable.

The response factors were calculated using the following equations[51]

$$RF = \frac{Abs_{gas} - Abs_{air}}{Abs_{gas}} \times 100\% \quad (5)$$

where Abs_{gas} and Abs_{air} are the absorbance in gas and air ambience, respectively. As the concentration of hydrogen gas increased from 0.06 to 1.0%, the response factor also increased from 2.8 to 12.1%.

The performances of the optical sensors under different hydrogen concentrations were further evaluated in terms of response and recovery time. The response time is defined as the time required for the variation in absorbance to reach 90% of the equilibrium absorbance peak value after a test gas was injected, and the recovery time as the time necessary for the sensor to return to 10% above the equilibrium absorbance peak value in air after releasing the test gas.[51] Figure 9 shows the plot of response and recovery times under different concentrations of hydrogen gas exposure. It was found that, when the concentration of hydrogen increased, the response time decreased. However, the sensor required a longer time to recover when the hydrogen concentration was increased.

In general, the response time of the sensors is much shorter than the recovery time. Hydrogen gas concentrations of 0.06, 0.12, 0.25, 0.5 and 1.0% result in response times of 62, 52, 45, 32, and 12 s, while recovery times were 190, 212, 225, 259, and 275 s. It can be concluded that the nanoporous anodic Pt/Nb_2O_5 sensing element performance exhibited a strong

DOI: 10.1021/am508463g
ACS Appl. Mater. Interfaces 2015, 7, 4751−4758

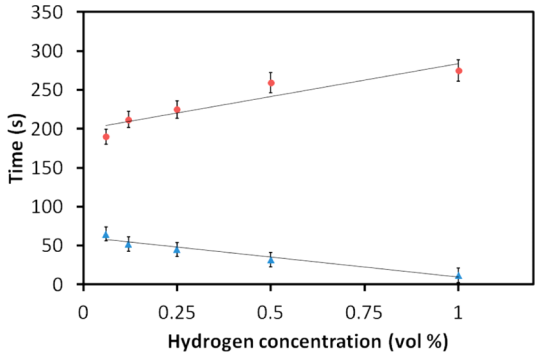

Figure 9. Plot of response and recovery times at various hydrogen gas concentrations for a nanoporous anodic Pt/Nb_2O_5 sensing element at 100 °C.

dependence on the hydrogen gas concentration. With the increased hydrogen gas concentration, the adsorption of H^+ ions is high; thereby favoring fast electron injection and H^+ intercalation into the nanoporous Nb_2O_5 films and therefore enhanced response times (a discussion regarding the diffusion depth of the gas molecules is presented in the Supporting Information). However, it is suggested that the increase in hydrogen gas concentration also results in large changes in the film stoichiometry, and therefore restoring the film to its initial state will take longer.

For benchmarking and in order to investigate the selectivity of the sensing elements, further experiments were conducted. The film was exposed to ethanol and methane gas at 1% concentration, and the responses are shown in Figure 10. The

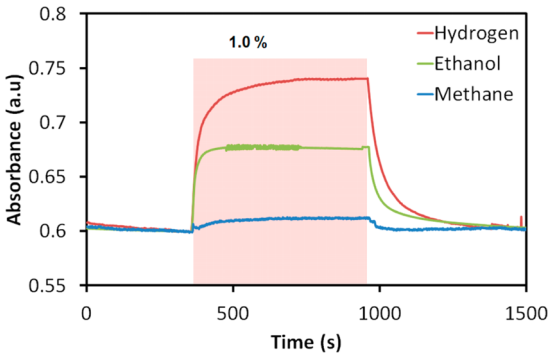

Figure 10. Absorbance change of the nanoporous anodic Pt/Nb_2O_5 sensing element in the presence of either 1% hydrogen, ethanol, or methane at an operating temperature of 100 °C.

absorbance change under ethanol vapor exposure was slightly lower than that of hydrogen gas. However, the exposure to methane gas resulted in a relatively smaller absorbance change. Thus, the Nb_2O_5 sensing element exhibited stronger interactions to ethanol and hydrogen molecules in comparison to methane.

Altogether, this optical system offers a number of advantages over the electrical based units incorporating similar nanoporous anodic Nb_2O_5 sensitive films. In comparison to our previous work,[52] in which the sensing performance of a Schottky-based anodic Nb_2O_5 hydrogen gas sensor was investigated, the relative absorbance change in response to hydrogen gas is slightly higher in this case. Additionally, the operating temperature of this optical system is also lower than our previously reported Schottky based gas sensor.

CONCLUSIONS

In this work, we successfully demonstrated the possibility of using nanoporous anodic Nb_2O_5 films for optical hydrogen gas sensing. These films were obtained using a high temperature anodization technique in a glycerol based electrolyte at 180 °C that resulted in Nb_2O_5 nanostructures. In the gas sensing experiments, the hydrogen gas molecules are dissociated into H^+ ions in a processes facilitated by a thin Pt layer. The intercalation of H^+ into the nanoporous anodic Nb_2O_5 films altered their electronic band structure, thereby exhibiting an absorption change which contributed to the sensor's response. The optical absorbance measurements upon exposure to hydrogen gas were conducted at temperatures starting from room temperature to 100 °C. The nanoporous films of ~500 nm thickness with a high active surface area demonstrated modest absorbance changes at 100 °C with a response factor of 12.1% when exposed to 1% hydrogen in ambient air as well as a rapid response and recovery. The presented work is the first report on hydrogen sensing behavior using optical modulation of nanoporous anodic Nb_2O_5 sensing elements, and future investigations are required to reveal their applications for sensing other gas species.

ASSOCIATED CONTENT

Supporting Information

A figure showing the optical gas sensing measurement setup, the calculations of the optical band gap in the presence of air and hydrogen using the Tauc equation, and discussion on the thickness effect of nanoporous anodic Nb_2O_5 in the gas sensing process. This material is available free of charge via the Internet at http://pubs.acs.org.

AUTHOR INFORMATION

Corresponding Authors

*E-mail: rosmalini@gmail.com.

*Phone: +61-3-99253254. Fax: +61-3-99253242. E-mail: kourosh.kalantar@rmit.edu.au.

Notes

The authors declare no competing financial interest.

ACKNOWLEDGMENTS

The authors acknowledge the facilities, and the scientific and technical assistance, of the Australian Microscopy & Microanalysis Research Facility at the RMIT Microscopy & Microanalysis Facility (RMMF), at RMIT University. The authors also would like to acknowledge Ministry of Education (MOE), Malaysia for the financial assistance.

REFERENCES

(1) Ou, J. Z.; Balendhran, S.; Field, M. R.; McCulloch, D. G.; Zoolfakar, A. S.; Rani, R. A.; Zhuiykov, S.; O'Mullane, A. P.; Kalantar-zadeh, K. The Anodized Crystalline WO_3 Nanoporous Network with Enhanced Electrochromic Properties. *Nanoscale* **2012**, *4*, 5980−5988.

(2) Di Yao, D.; Field, M. R.; O'Mullane, A. P.; Kalantar-zadeh, K.; Ou, J. Z. Electrochromic Properties of TiO_2 Nanotubes Coated with Electrodeposited MoO_3. *Nanoscale* **2013**, *5*, 10353−10359.

(3) Ou, J. Z.; Yaacob, M. H.; Breedon, M.; Zheng, H. D.; Campbell, J. L.; Latham, K.; du Plessis, J.; Wlodarski, W.; Kalantar-zadeh, K. In Situ Raman Spectroscopy of H_2 Interaction with WO_3 Films. *Phys. Chem. Chem. Phys.* **2011**, *13*, 7330−7339.

(4) Zheng, H.; Ou, J. Z.; Strano, M. S.; Kaner, R. B.; Mitchell, A.; Kalantar-zadeh, K. Nanostructured Tungsten Oxide - Properties, Synthesis, and Applications. *Adv. Funct. Mater.* **2011**, *21*, 2175−2196.

DOI: 10.1021/am508463g
ACS Appl. Mater. Interfaces 2015, 7, 4751−4758

(5) Yaacob, M. H.; Yu, J.; Latham, K.; Kalantar-zadeh, K.; Wlodarski, W. Optical Hydrogen Sensing Properties of Nanostructured Pd/MoO_3 Films. *Sens. Lett.* **2011**, *9*, 16−20.
(6) Yao, D. D.; Ou, J. Z.; Latham, K.; Zhuiykov, S.; O'Mullane, A. P.; Kalantar-zadeh, K. Electrodeposited α- and β-Phase MoO_3 Films and Investigation of Their Gasochromic Properties. *Cryst. Growth Des.* **2012**, *12*, 1865−1870.
(7) Aegerter, M. Sol-Gel Chromogenic Materials and Devices. In *Optical and Electronic Phenomena in Sol-Gel Glasses and Modern Application*; Springer: Berlin, Heidelberg, 1996; Vol. *85*, pp 149−194.
(8) Korosec, R. C.; Bukovec, P. Sol-Gel Prepared NiO Thin Films for Electrochromic Applications. *Acta Chim. Slov.* **2006**, *53*, 136−147.
(9) Niklasson, G. A.; Granqvist, C. G. Electrochromics for Smart Windows: Thin Films of Tungsten Oxide and Nickel Oxide, and Devices Based on These. *J. Mater. Chem.* **2007**, *17*, 127−156.
(10) Moulki, H.; et al. Electrochromic Performances of Non-stoichiometric NiO Thin Films. *Thin Solid Films* **2014**, *553*, 63−66.
(11) Romero, R.; Dalchiele, E. A.; Martin, F.; Leinen, D.; Ramos-Barrado, J. R. Electrochromic Behaviour of Nb_2O_5 Thin Films with Different Morphologies Obtained by Spray Pyrolysis. *Sol. Energy Mater. Sol. C* **2009**, *93*, 222−229.
(12) Rosario, A. V.; Pereira, E. C. Optimisation of the Electrochromic Properties of Nb_2O_5 Thin Films Produced by Sol-Gel Route Using Factorial Design. *Sol. Energy Mater. Sol. C* **2002**, *71*, 41−50.
(13) Yao, D. D.; Rani, R. A.; O'Mullane, A. P.; Kalantar-zadeh, K.; Ou, J. Z. High Performance Electrochromic Devices Based on Anodized Nanoporous Nb_2O_5. *J. Phys. Chem. C* **2014**, *118*, 476−481.
(14) Verma, A.; Singh, P. K. Sol-Gel Derived Nanostructured Niobium Pentoxide Thin Films for Electrochromic Applications. *Indian J. Chem., Sect. A* **2013**, *52*, 593−598.
(15) Lee, G. R.; Crayston, J. A. Electrochromic Nb_2O_5 and Nb_2O_5/Silicone Composite Thin Films Prepared by Sol-Gel Processing. *J. Mater. Chem.* **1991**, *1*, 381−386.
(16) Yoshimura, K.; Miki, T.; Tanemura, S. Electrochromic Properties of Niobium Oxide Thin Films Prepared by Dc Magnetron Sputtering. *J. Electrochem. Soc.* **1997**, *144*, 2982−2985.
(17) Yoshimura, K.; Miki, T.; Iwama, S.; Tanemura, S. Niobium Oxide Electrochromic Thin-Films Prepared by Reactive Dc Magnetron Sputtering. *Jpn. J. Appl. Phys., Part 2* **1995**, *34*, L1293−L1296.
(18) Orel, B.; Macek, M.; Grdadolnik, J.; Meden, A. In Situ Uv-Vis and Ex Situ Ir Spectroelectrochemical Investigations of Amorphous and Crystalline Electrochromic Nb_2O_5 Films in Charged/Discharged States. *J. Solid State Electrochem.* **1998**, *2*, 221−236.
(19) Hu, W.; Liu, Z.; Tian, D.; Zhang, S.; Zhao, Y.; Yao, K. Morphological Evolution of Nb_2O_5 in a Solvothermal Reaction: From Nb_2O_5 Grains to Nb_2O_5 Nanorods and Hexagonal Nb_2O_5 Nanoplatelets. *J. Wuhan Univ. Technol.* **2009**, *24*, 245−248.
(20) Fang, X.; Hu, L.; Huo, K.; Gao, B.; Zhao, L.; Liao, M.; Chu, P. K.; Bando, Y.; Golberg, D. New Ultraviolet Photodetector Based on Individual Nb_2O_5 Nanobelts. *Adv. Funct. Mater.* **2011**, *21*, 3907−3915.
(21) Wei, M.; Qi, Z.-m.; Ichihara, M.; Zhou, H. Synthesis of Single-Crystal Niobium Pentoxide Nanobelts. *Acta Mater.* **2008**, *56*, 2488−2494.
(22) Luo, H.; Wei, M.; Wei, K. Synthesis of Nb_2O_5 Nanorods by a Soft Chemical Process. *J. Nanomater.* **2009**, 758353.
(23) Luo, H.; Wei, M.; Wei, K. Synthesis of Nb_2O_5 Nanosheets and Its Electrochemical Measurements. *Mater. Chem. Phys.* **2010**, *120*, 6−9.
(24) Zhao, Y.; Eley, C.; Hu, J.; Foord, J. S.; Ye, L.; He, H.; Tsang, S. C. E. Shape-Dependent Acidity and Photocatalytic Activity of Nb_2O_5 Nanocrystals with an Active TT (001) Surface. *Angew. Chem., Int. Ed.* **2012**, *51*, 3846−3849.
(25) Rani, R. A.; Zoolfakar, A. S.; Subbiah, J.; Ou, J. Z.; Kalantar-zadeh, K. Highly Ordered Anodized Nb_2O_5 Nanochannels for Dye-Sensitized Solar Cells. *Electrochem. Commun.* **2014**, *40*, 20−23.
(26) Rani, R. A.; Zoolfakar, A. S.; Ou, J. Z.; Field, M. R.; Austin, M.; Kalantar-zadeh, K. Nanoporous Nb_2O_5 Hydrogen Gas Sensor. *Sens. Actuators, B* **2013**, *176*, 149−156.
(27) Rahman, M. M.; Rani, R. A.; Sadek, A. Z.; Zoolfakar, A. S.; Field, M. R.; Ramireddy, T.; Kalantar-zadeh, K.; Chen, Y. A Vein-Like Nanoporous Network of Nb_2O_5 with a Higher Lithium Intercalation Discharge Cut-Off Voltage. *J. Mater. Chem. A* **2013**, *1*, 11019−11025.
(28) Ou, J. Z.; et al. Elevated Temperature Anodized Nb_2O_5: A Photoanode Material with Exceptionally Large Photoconversion Efficiencies. *ACS Nano* **2012**, *6*, 4045−4053.
(29) Mozalev, A.; Vazquez, R. M.; Bittencourt, C.; Cossement, D.; Gispert-Guirado, F.; Llobet, E.; Habazaki, H. Formation-Structure-Properties of Niobium-Oxide Nanocolumn Arrays Via Self-Organized Anodization of Sputter-Deposited Aluminum-on-Niobium Layers. *J. Mater. Chem. C* **2014**, *2*, 4847−4860.
(30) Lee, K.; Yang, Y.; Yang, M.; Schmuki, P. Formation of Highly Ordered Nanochannel Nb Oxide by Self-Organizing Anodization. *Chem.—Eur. J.* **2012**, *18*, 9521−9524.
(31) Wang, H.; et al. Electrochemical Tuning of Vertically Aligned MoS_2 Nanofilms and Its Application in Improving Hydrogen Evolution Reaction. *Proc. Natl. Acad. Sci. U. S. A.* **2013**, *110*, 19701−19706.
(32) Deb, S. K. Reminiscences on the Discovery of Electrochromic Phenomena in Transition Metal Oxides. *Sol. Energy Mater. Sol. C* **1995**, *39*, 191−201.
(33) Granqvist, C. G. Electrochromic Tungsten Oxide Films: Review of Progress 1993−1998. Sol. *Energy Mater. Sol. C* **2000**, *60*, 201−262.
(34) Gillaspie, D. T.; Tenent, R. C.; Dillon, A. C. Metal-Oxide Films for Electrochromic Applications: Present Technology and Future Directions. *J. Mater. Chem.* **2010**, *20*, 9585−9592.
(35) Yao, D. D.; Rani, R. A.; O'Mullane, A. P.; Kalantar-zadeh, K.; Ou, J. Z. Enhanced Coloration Efficiency for Electrochromic Devices Based on Anodized Nb_2O_5/Electrodeposited MoO_3 Binary Systems. *J. Phys. Chem. C* **2014**, *118*, 10867−10873.
(36) Momirlan, M.; Veziroglu, T. N. The Properties of Hydrogen as Fuel Tomorrow in Sustainable Energy System for a Cleaner Planet. *Int. J. Hydrogen Energy* **2005**, *30*, 795−802.
(37) Hart, D. Hydrogen End Uses and Economics. In *Encyclopedia of Energy*; Cleveland, C. J., Ed.; Elsevier: New York, 2004; pp 231−239.
(38) Dunn, S. History of Hydrogen. In *Encyclopedia of Energy*; Cleveland, C. J., Ed.; Elsevier: New York, 2004; pp 241−252.
(39) Ramachandran, R.; Menon, R. K. An Overview of Industrial Uses of Hydrogen. *Int. J. Hydrogen Energy* **1998**, *23*, 593−598.
(40) Huebert, T.; Boon-Brett, L.; Black, G.; Banach, U. Hydrogen Sensors - a Review. *Sens. Actuators, B Chem.* **2011**, *157*, 329−352.
(41) Melody, B.; Kinard, T.; Lessner, P. The Non-Thickness-Limited Growth of Anodic Oxide Films on Valve Metals. *Electrochem. Solid-State Lett.* **1998**, *1*, 126−129.
(42) Truong Nhat, N.; Kim, D.; Jeong, D.-Y.; Kim, M.-W.; Kim, J. U. Formation Behavior of Nanoporous Anodic Aluminum Oxide Films in Hot Glycerol/Phosphate Electrolyte. *Electrochim. Acta* **2012**, *83*, 288−293.
(43) Yang, S.; Aoki, Y.; Habazaki, H. Effect of Electrolyte Temperature on the Formation of Self-Organized Anodic Niobium Oxide Microcones in Hot Phosphate-Glycerol Electrolyte. *Appl. Surf. Sci.* **2011**, *257*, 8190−8195.
(44) Lu, Q.; Hashimoto, T.; Skeldon, P.; Thompson, G. E.; Habazaki, H.; Shimizu, K. Nanoporous Anodic Niobium Oxide Formed in Phosphate/Glycerol Electrolyte. *Electrochem. Solid-State Lett.* **2005**, *8*, B17−B20.
(45) Oikawa, Y.; Minami, T.; Mayama, H.; Tsujii, K.; Fushimi, K.; Aoki, Y.; Skeldon, P.; Thompson, G. E.; Habazaki, H. Preparation of Self-Organized Porous Anodic Niobium Oxide Microcones and Their Surface Wettability. *Acta Mater.* **2009**, *57*, 3941−3946.
(46) Dacca, A.; Gemme, G.; Mattera, L.; Parodi, R. XPS Analysis of the Surface Composition of Niobium for Superconducting Rf Cavities. *Appl. Surf. Sci.* **1998**, *126*, 219−230.
(47) Brayner, R.; Bozon-Verduraz, F. Niobium Pentoxide Prepared by Soft Chemical Routes: Morphology, Structure, Defects and Quantum Size Effect. *Phys. Chem. Chem. Phys.* **2003**, *5*, 1457−1466.
(48) Hyodo, T.; Ohoka, J.; Shimizu, Y.; Egashira, M. Design of Anodically Oxidized Nb_2O_5 Films as a Diode-Type H_2 Sensing Material. *Sens. Actuators, B* **2006**, *117*, 359−366.

DOI: 10.1021/am508463g
ACS Appl. Mater. Interfaces 2015, 7, 4751−4758

(49) Yaacob, M. H.; Ahmad, M. Z.; Sadek, A. Z.; Ou, J. Z.; Campbell, J.; Kalantar-zadeh, K.; Wlodarski, W. Optical Response of WO_3 Nanostructured Thin Films Sputtered on Different Transparent Substrates Towards Hydrogen of Low Concentration. *Sens. Actuators, B* **2013**, *177*, 981−988.
(50) Hübert, T.; Boon-Brett, L.; Black, G.; Banach, U. Hydrogen Sensors − a Review. *Sens. Actuators, B* **2011**, *157*, 329−352.
(51) Alsaif, M. M. Y. A.; Field, M. R.; Murdoch, B. J.; Daeneke, T.; Latham, K.; Chrimes, A. F.; Zoolfakar, A. S.; Russo, S. P.; Ou, J. Z.; Kalantar-zadeh, K. Substoichiometric Two-Dimensional Molybdenum Oxide Flakes: A Plasmonic Gas Sensing Platform. *Nanoscale* **2014**, *6*, 12780−12791.
(52) Kadir, R. A.; Rani, R. A.; Zoolfakar, A. S.; Ou, J. Z.; Shafiei, M.; Wlodarski, W.; Kalantar-zadeh, K. Nb_2O_5 Schottky Based Ethanol Vapour Sensors: Effect of Metallic Catalysts. *Sens. Actuators, B* **2014**, *202*, 74−82.

DOI: 10.1021/am508463g
ACS Appl. Mater. Interfaces 2015, 7, 4751−4758